Displacements and stress distribution in D0 Run IIb stave due to CTE mismatches

Giobatta Lanfranco, James Fast

Fermi National Accelerator Laboratory
Particle Physics Division / Silicon Engineering Group - Mechanical Dep.
e-mail: giobatta@fnal.gov , jfast@fnal.gov

24 July 2001

1. Abstract

A possible D0 Run IIb stave design currently under study is characterized by an outer carbon fiber stiffening shell with the silicon detectors mounted internally and a single central cooling line running between them; in this paper the stave will be analyzed for thermal compatibility since the different coefficient of thermal expansion in the materials may cause unpredictable stresses and strains in the structure. A simplified stave section has been modeled with finite elements for different materials configurations and the vertical and longitudinal displacements induced by the thermal gradient, together with the related stresses, have been computed. Finally, once selected the most suitable material combination, a more realistic model has been created in order to study the influence of the hybrid location along the ladders.

2. Stave layout

The stave is constructed from 200mm long ladders consisting of two silicon sensors, 37.2 mm wide by 100 mm long, glued together end-to-end with a hybrid, 35 mm wide and 60 mm long, glued to the silicon, centered on the sensor to sensor joint. Six of these ladder structures are joined end-to-end to form a 1.2m long chain and two chains are attached to opposite sides of the stave core and cooling lines. Each hybrid has 10 SVX chips mounted on it for a total heat load of 5W per hybrid. Because of the way the silicon sensors are ganged together, the hybrids may be spaced facing each other or in alternate order; these two configurations with their asymmetry may induce higher thermal gradient related displacements and have been investigated at the end of the present paper.

The 1.2 m long silicon chains are bonded to either side of the core with axial strip readout on one side and small angle stereo strip readout on the other. Finally, two composite C-channels are attached around the silicon to form a box structure that provides most of the stave stiffness. The stave length is 48" (1.22m) with support provided at the center and the two ends. The silicon supporting blocks are equally spaced and are 2 mm high x 4 mm long x 8 mm wide.

Figure 1 shows a cross-section of the stave. Table 1 summarizes the stave constituent materials, their thickness and their thermal conductivities.

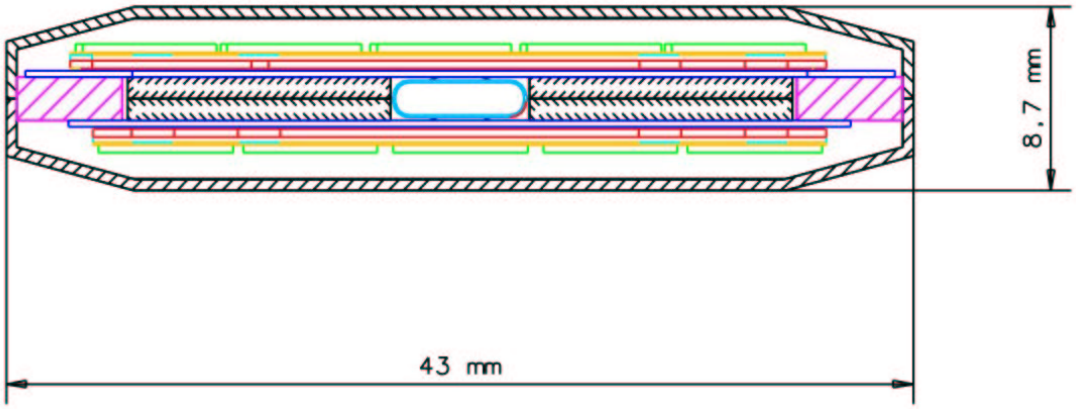

Figure 1 – The ladder section

Component	**material**	**Thickness [μm]**	**Thermal conductivity [W/mK]**	**Color code in Figure 1**
Support shell	*investigated*	500	-	black
Sensor	Silicon	380	124	blue
Chip	Silicon	300	124	green
Glue	Epoxy	50	1	*not depicted*
Tubing	PEEK	100	0.25	cyan
HDI	Kapton	100	0.2	gold
Substrate	BeO	500	250	red
Heat spreader	*investigated*	100	-	*not depicted*
Core	Rohacell	2000	~ 0	black (short hatch)
Support block	ceramic	2000	1.46	magenta

Table 1 - Thermal conductivities and thickness of the stave constituent materials

3. Finite element models

The model analyzed is constituted by a C shaped shell supporting a silicon sensor glued to a heat spreader. The material of the shell structure and of the heat spreader, as well as the number of the supports, have been varied so to have the following six configurations:

Case	Shell	Heat Spreader	Core	Supports
1	K139 + Boron prepreg[1]	hypothetical	-	4
2	K139 + Boron prepreg[1]	kapton	-	4
3	K139 + Boron prepreg[1]	K13D2U[2]	-	4
4	K139 [90° - 0°][3]	K13D2U[2]	-	4
5	K139 [90° - 0°][3]	K13D2U[2]	-	6
6	K139 [90° - 0°][3]	K13D2U[2]	Rohacell	6

Table 2 – Finite element models studied

The K139 + Boron prepreg closely matches the coefficient of thermal expansion (CTE) of silicon along the longitudinal direction (z), so that no stresses are introduced in the sensor. The K139 [90°-0°] offers instead higher mechanical properties and presents no significant longitudinal elongation[4], with the advantage of an easier stave anchoring.

The heat spreader, although the misleading name, has the main function to help with assembling and handling the silicon sensor chain; that explains the choice of testing kapton although its poor thermal conductivity (*K*). K13D2U shows a similar low inter-laminar thermal conductivity, since in the through-plane direction the heat transfer is mainly relying on the resin. However a K13D2U heat spreader is preferable to kapton for its better mechanical properties and for the fact that the higher transversal and longitudinal values of K facilitate spreading the heat to regions at lower heat density giving a smoother temperature gradient distribution.

The hypothetical material in the heat spreader of case 1 is a substance perfectly matching CTE and elastic modulus of silicon.

[1] See Table 3.

[2] See Table 5.

[3] See Table 4.

[4] Because of its virtually zero CTE.

The supports are small ceramic blocks and are thought perfectly fixed to the Silicon. No glue has been modeled except at the interface between silicon and heat spreader and between heat spreader and Rohacell (configuration 6).

From Table 3 to Table 5 the properties of the carbon fiber laminates are shown. In Table 6 the Young's modulus and the CTE of the materials used are given.

Boron 5505/4 + k139-1515-70/30

Ply #	Lamina Type	Thickness	Angle
1	k139-1515-70/30	55	54
2	Boron 5505/4	135	0
3	k139-1515-70/30	55	-54
4	k139-1515-70/30	55	-54
5	Boron 5505/4	135	0
6	k139-1515-70/30	55	54

Ex (pa)	106.2 GPa
Ey (pa)	77.5 GPa
Ez (pa)	15.7 GPa
Gxy (pa)	46.9 GPa
Gxz (pa)	0.8 GPa
Gyz (pa)	0.9 GPa
NUxy	0.49
NUyx	0.36
NUxz	0.14
NUzx	0.02
NUyz	0.31
NUzy	0.06
CTEx	2.50E-06 mm/mm/°C
CTEy	1.03E-07 mm/mm/°C
CTEz	3.31E-05 mm/mm/°C
Density	1.875 g/cm³
Thickness	490 Micron

Table 3 - Lay-up and properties of the laminate containingK139 and boron prepreg

K139 [90° - 0°]

# Plies	Fiber type	Resin Type	Resin to Fiber ratio	Thickness [μm]	Angle Layout
7	Mitsubishi K139	EX 1515	70/30	75	90°-0°-90°-0°-90°-0°-90°

Ex (pa)	185	GPa
Ey (pa)	245	GPa
Ez (pa)	8.4	GPa
Gxy (pa)	2.2	GPa
Gxz (pa)	1.7	GPa
Gyz (pa)	1.8	GPa
NUxy	7.7×10^{-3}	
NUyx	1.02×10^{-2}	
NUxz	0.53	
NUzx	2.4×10^{-2}	
NUyz	0.52	
NUzy	1.8×10^{-2}	
CTEx	-7.5×10^{-7}	mm/mm/°C
CTEy	-9.25×10^{-7}	mm/mm/°C
CTEz	3.41×10^{-5}	mm/mm/°C
Density	1.714	g/cm³
Thickness	525	μm

Table 4 - Lay-up and properties of the laminate containingK139 [90° - 0°]

K13D2U

# Plies	Fiber type	Resin Type	Resin to Fiber ratio	Thickness [μm]	Angle Layout
3	Mitsubishi K13D2U	EX 1515	70/30	33	90°-0°-90°

Ex (pa)	176	GPa
Ey (pa)	346	GPa
Ez (pa)	8.4	GPa
Gxy (pa)	2.14	GPa
Gxz (pa)	1.59	GPa
Gyz (pa)	1.86	GPa
NUxy	5.48×10^{-3}	
NUyx	1.079×10^{-2}	
NUxz	0.55	
NUzx	2.625×10^{-2}	
NUyz	0.52	
NUzy	1.28×10^{-2}	
CTEx	-5×10^{-7}	mm/mm/°C
CTEy	-8.81×10^{-7}	mm/mm/°C
CTEz	3.46×10^{-5}	mm/mm/°C
Kx	147.5	W/m/K
Ky	295	W/m/K
Kz	0.3	W/m/K
Density	1.736	g/cm³
Thickness	99	μm

Table 5 - Lay-up and properties of the laminate containingK13D2U

Material	**CTE** [μm / m -°C]	**Young's modulus** [Gpa (Msi)]
Silicon	2.5	112.4 (16.3)
Kapton	20	2.8 (0.406)
Epoxy	43.8	3.2 (0.464)
Ceramic (MACOR)	7.4	66.9 (9.7)
Polyetheretherketone (PEEK)	40	3.8 (0.551)
Beryllia (BeO)	8.4	311 (45.1)
Rohacell 51 A	33	0.07 (0.01)

Table 6 – CTE and elastic modulus of materials used in the stave

In the following pictures (Figure 2 - Figure 13) it is possible to see the behaviour that the structure exhibits with a 30K temperature drop. Rohacell reduces the membrane behaviour of the silicon sensor and together with a third couple of supports half the span helps to greatly reduce the sag; the K13D2U heat spreader in conjunction with the K139 [90°-0°] restrain the silicon from elongating longitudinally. The stresses in the sensor never rise to a dangerous level, the safety factor always being at least five[5]. Table 7 summarizes the maximum and minimum values of vertical and longitudinal displacement and the longitudinal stress.

[5] The silicon compressive yield strength is about 120 MPa.

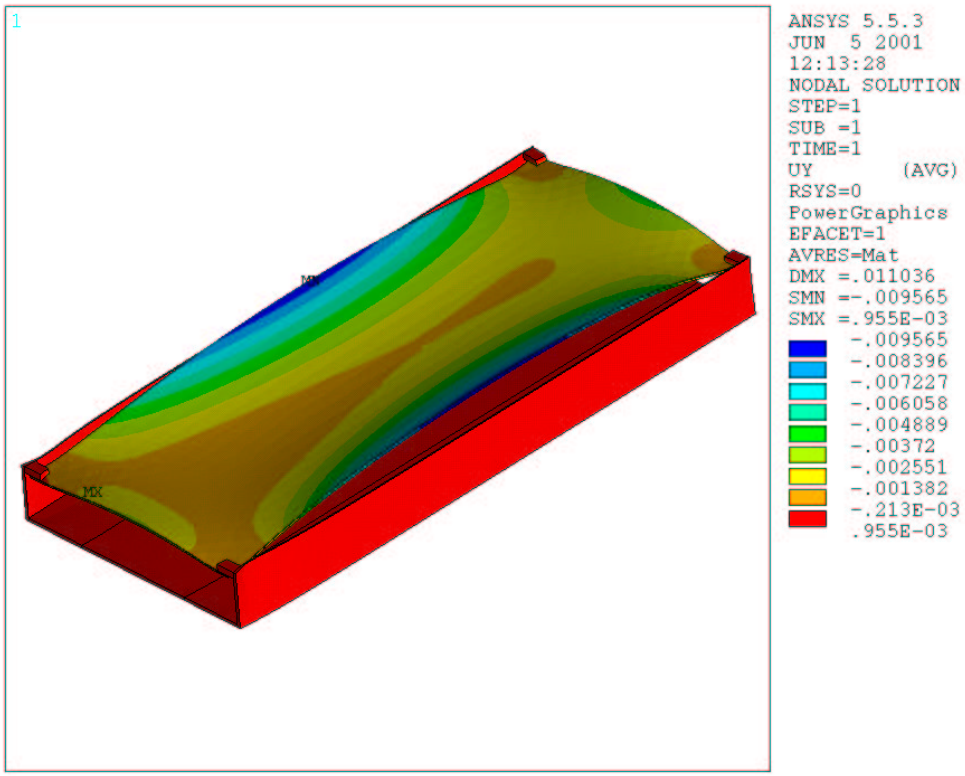

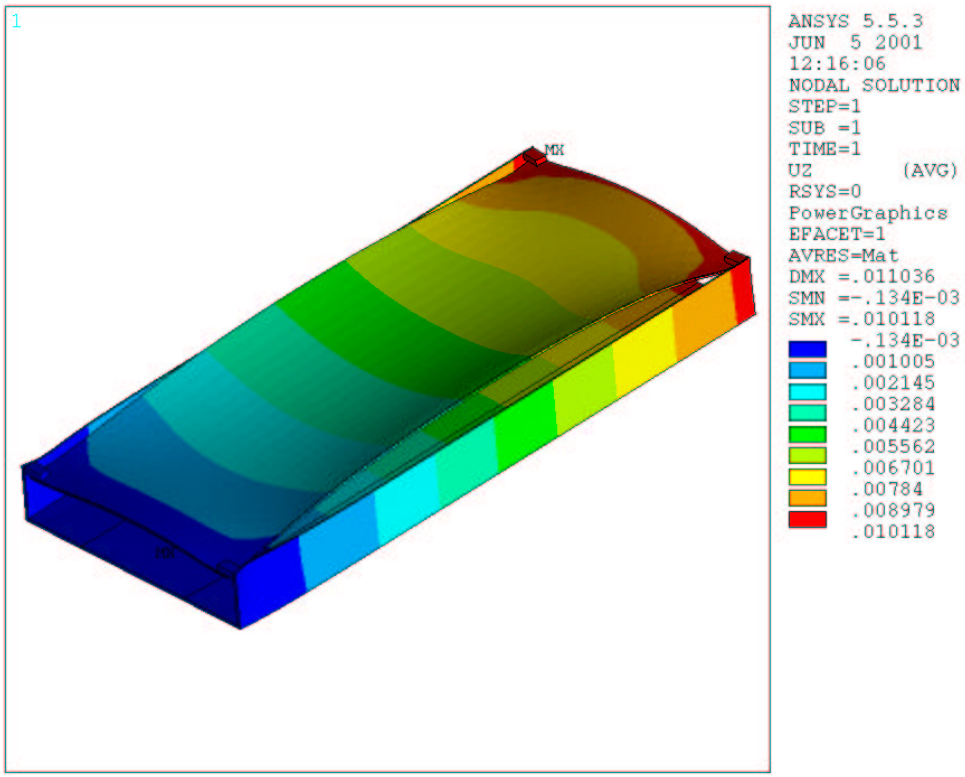

Figure 2 - From top to bottom: vertical and longitudinal displacements [mm] in half stave structure 100 mm long [Shell: K139 + Boron Prepreg; heat spreader perfectly matching silicon CTE]

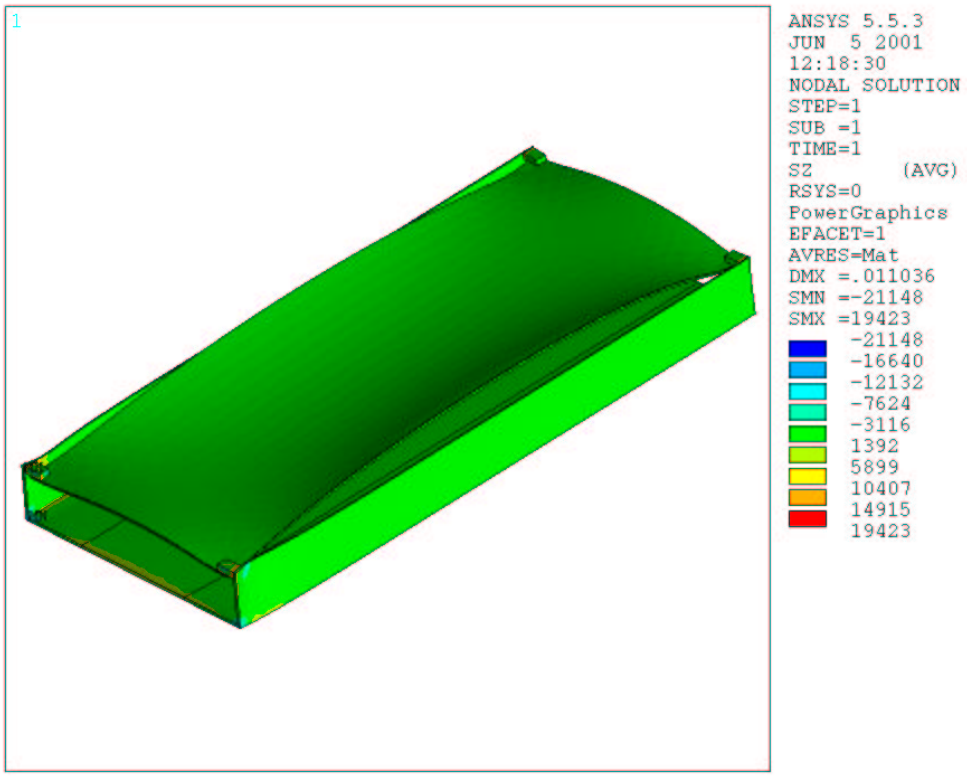

Figure 3 – Longitudinal stresses [kPa, ~1/7 psi] in half stave structure 100 mm long [Shell: K139 + Boron Prepreg; heat spreader perfectly matching silicon CTE]

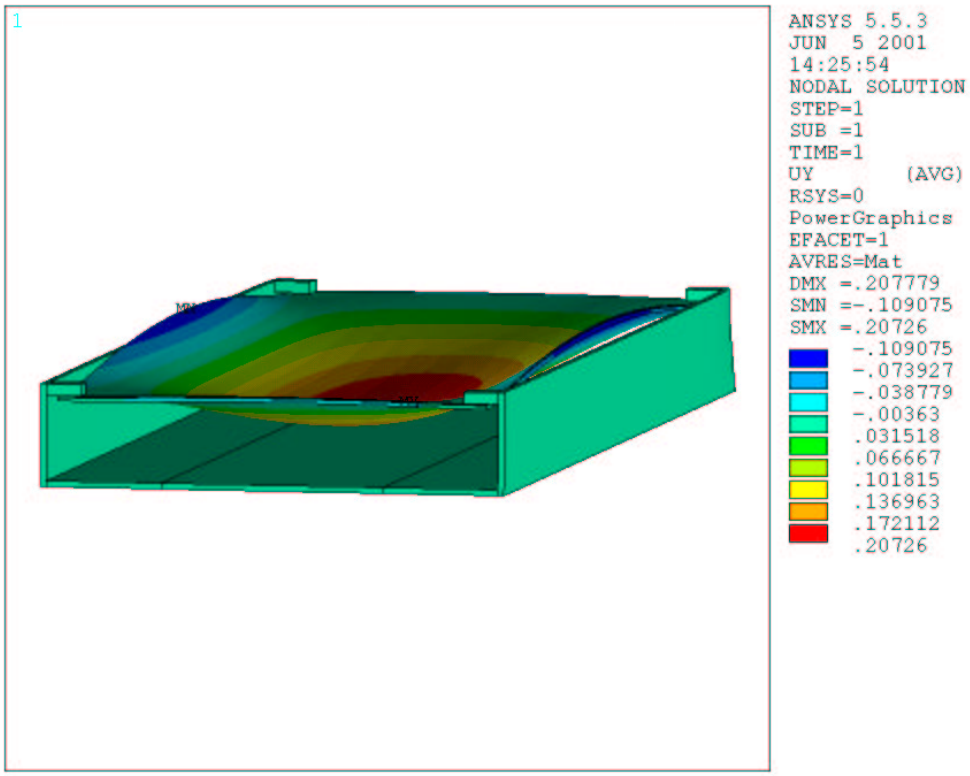

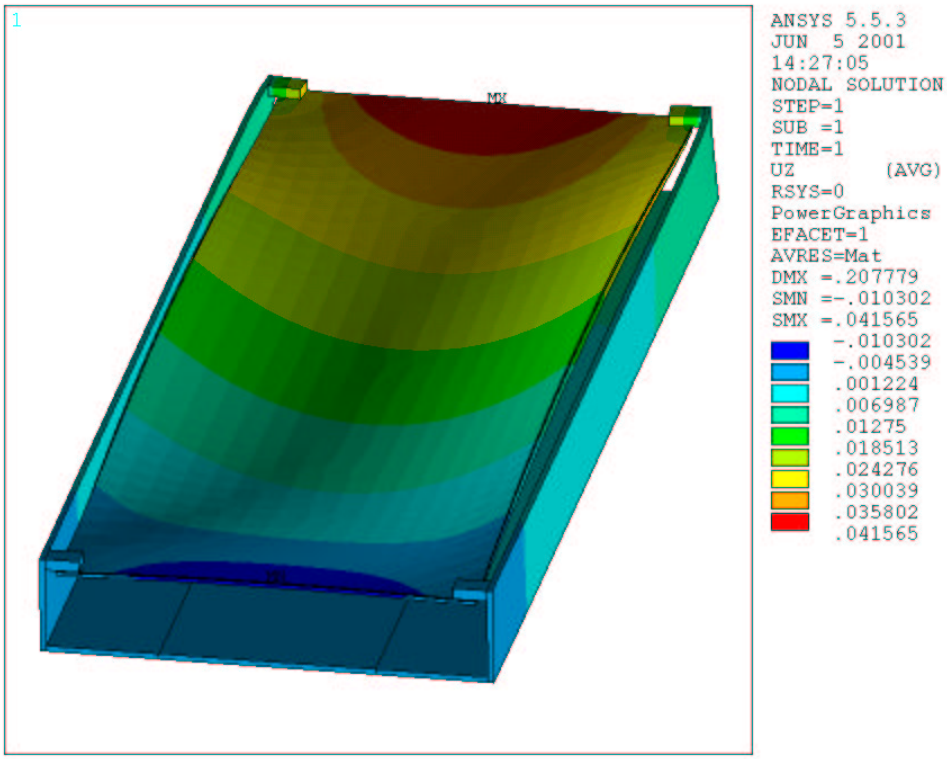

Figure 4 - From top to bottom: vertical and longitudinal displacements [mm] in half stave structure 100 mm long [Shell: K139 + Boron Prepreg; KAPTON heat spreader

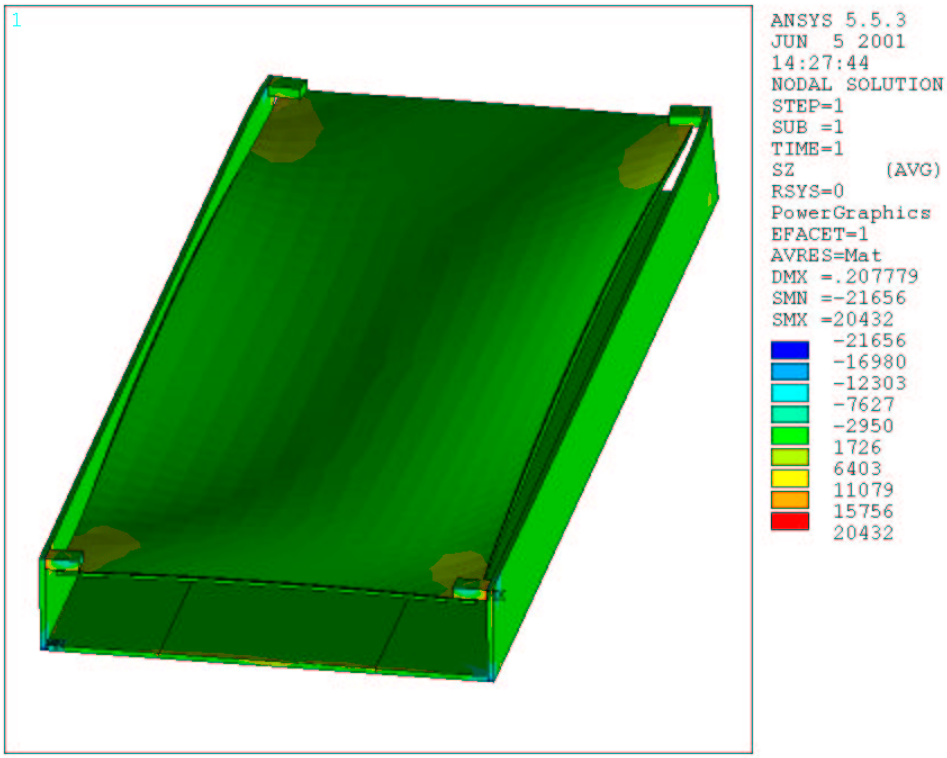

Figure 5 - Longitudinal stresses [kPa, ~1/7 psi] in half stave structure 100 mm long [Shell: K139 + Boron Prepreg; KAPTON heat spreader]

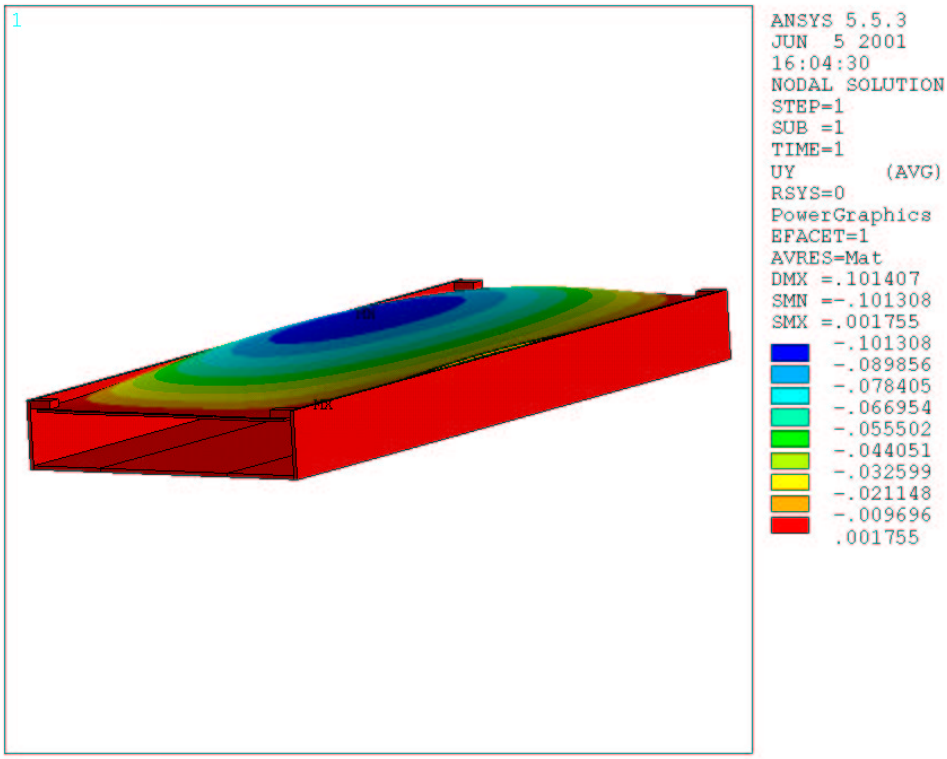

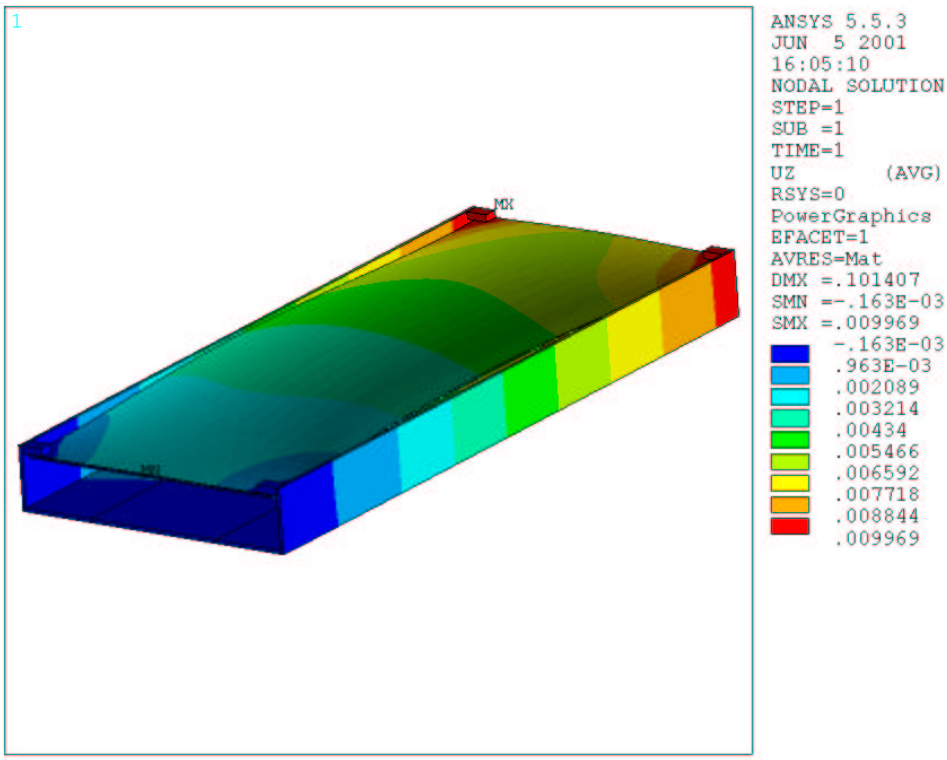

Figure 6 - From top to bottom: vertical and longitudinal displacements [mm] in half stave structure 100 mm long [Shell: K139 + Boron Prepreg; K13D2U heat spreader

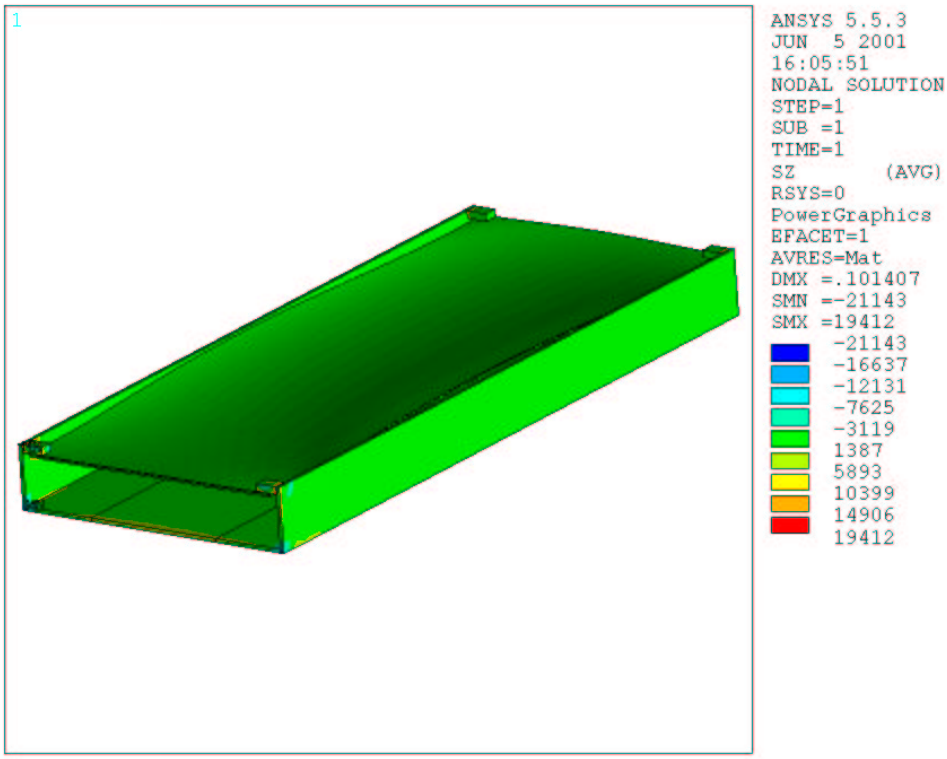

Figure 7 - Longitudinal stresses [kPa, ~1/7 psi] in half stave structure 100 mm long [Shell: K139 + Boron Prepreg; K13D2U heat spreader]

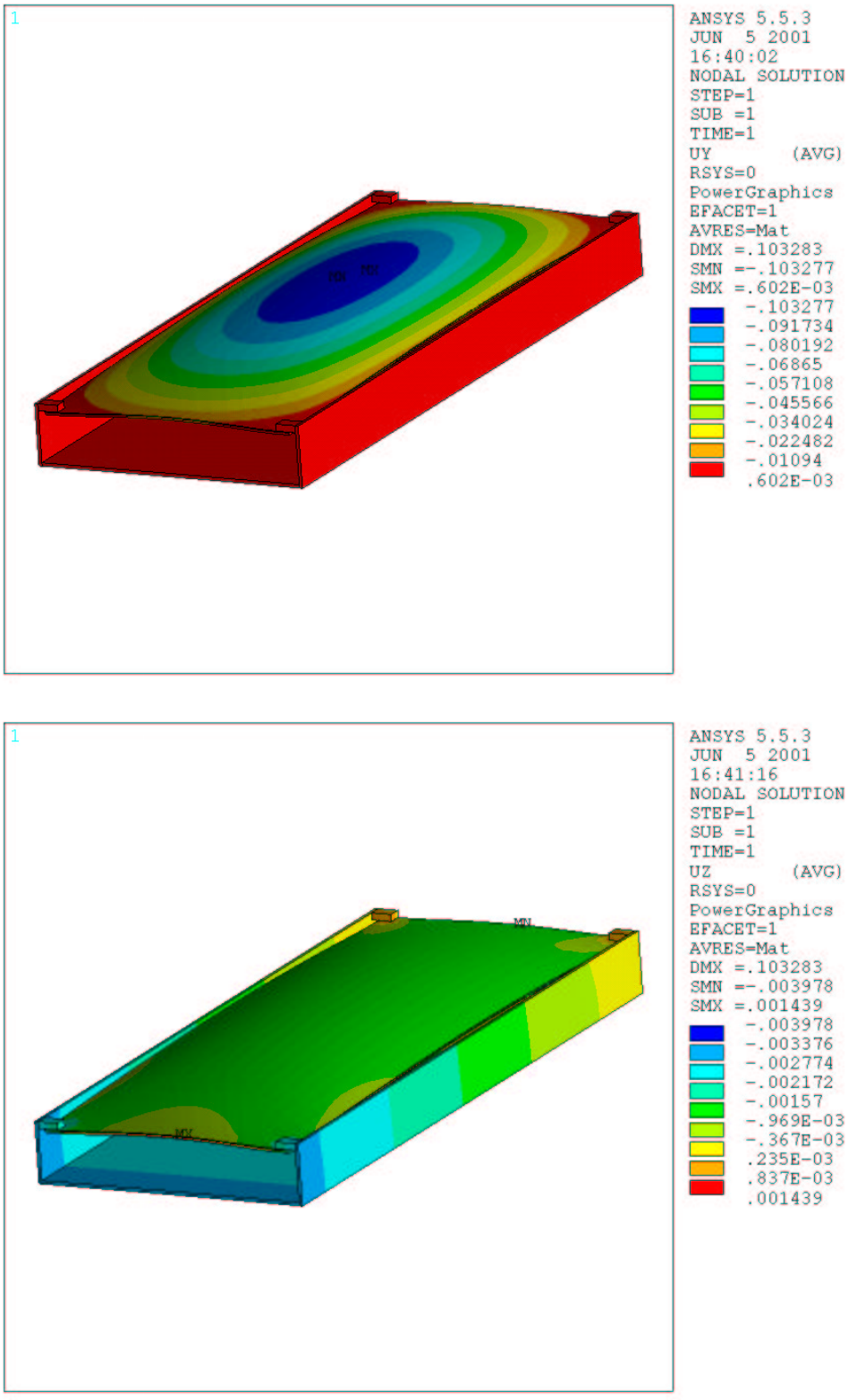

Figure 8 - From top to bottom: vertical and longitudinal displacements [mm] in half stave structure 100 mm long [Shell: K139 (90°-0°-90°-0°-90°-0°-90°); K13D2U heat spreader

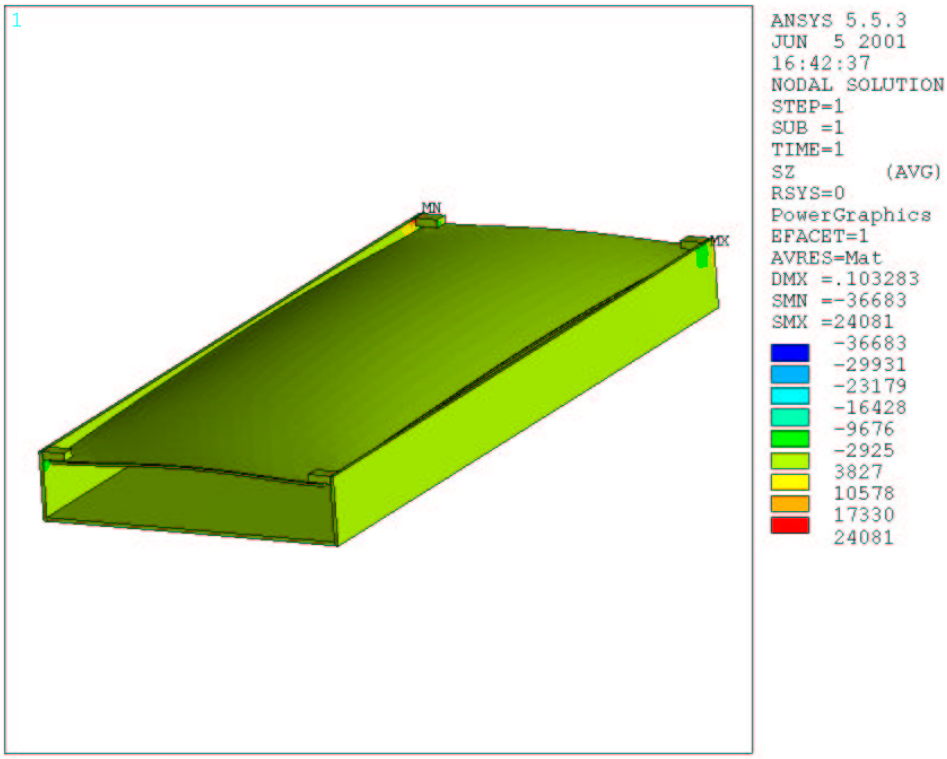

Figure 9 - Longitudinal stresses [kPa, ~1/7 psi] in half stave structure 100 mm long [Shell: K139 (90°-0°-90°-0°-90°-0°-90°); K13D2U heat spreader]

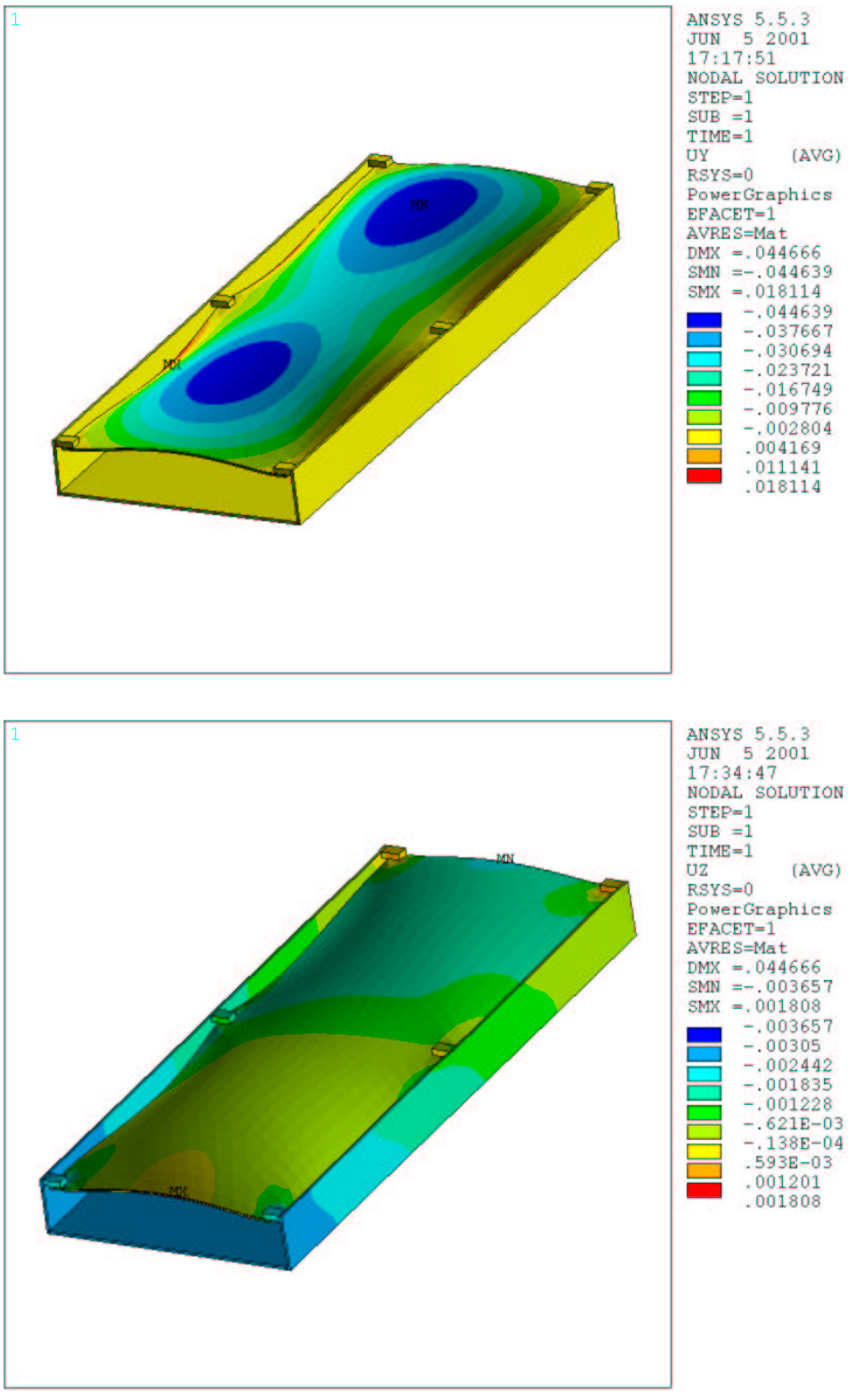

Figure 10 - From top to bottom: vertical and longitudinal displacements [mm] in half stave structure 100 mm long [Shell: K139 (90°-0°-90°-0°-90°-0°-90°); K13D2U heat spreader; 6 supports]

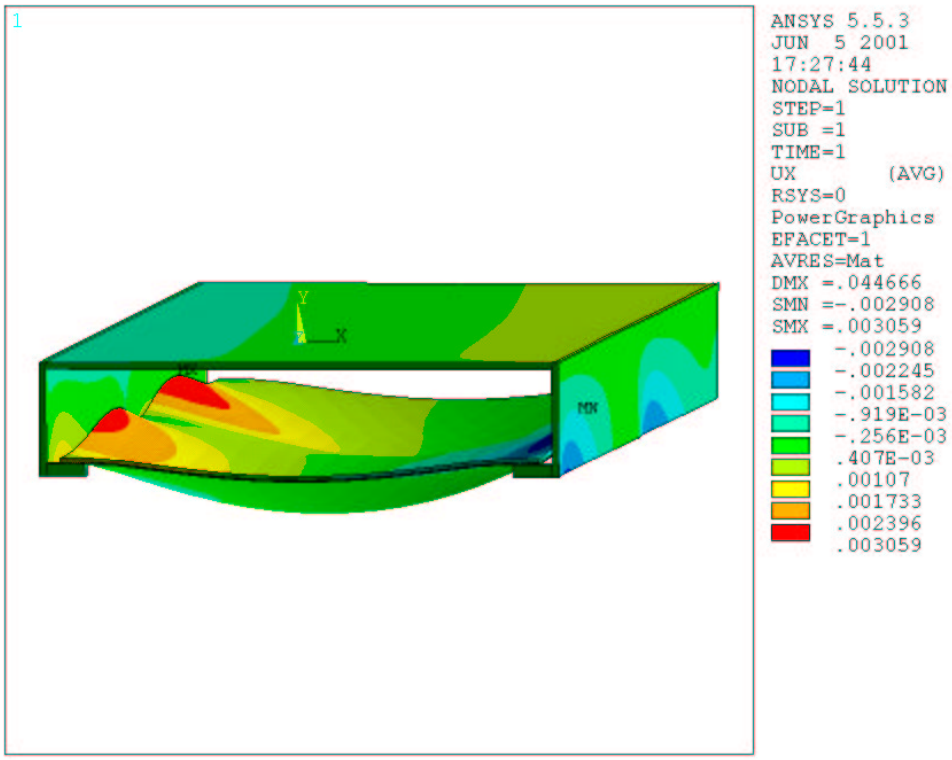

Figure 11 - Lateral displacements [mm] in half stave structure 100 mm long [Shell: K139 (90°-0°-90°-0°-90°-0°-90°); K13D2U heat spreader; 6 supports]

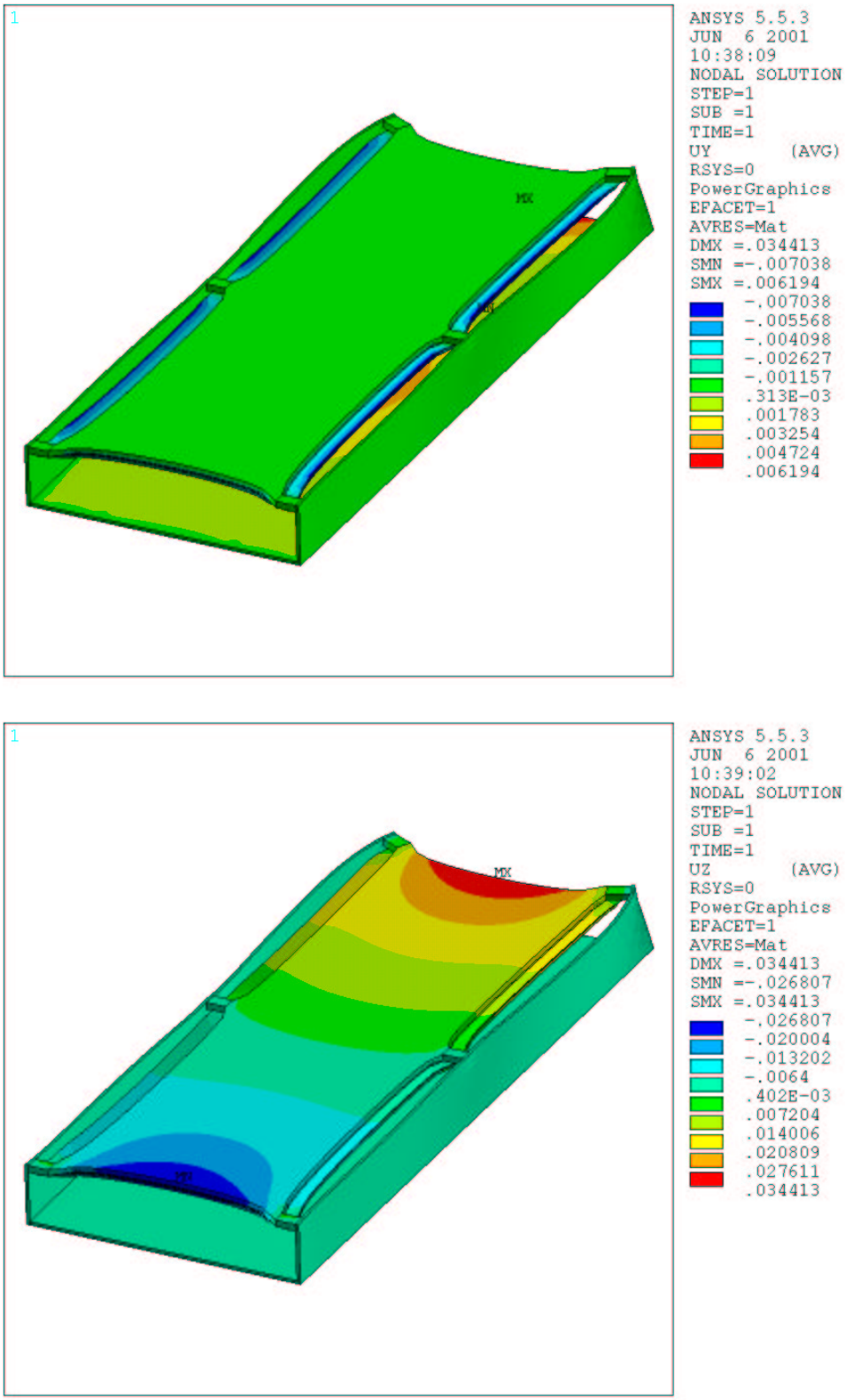

Figure 12 - From top to bottom: vertical and longitudinal displacement [mm] in half stave structure 100 mm long [Shell: K139 (90°-0°-90°-0°-90°-0°-90°); K13D2U heat spreader; Rohacell core; 6 supports]

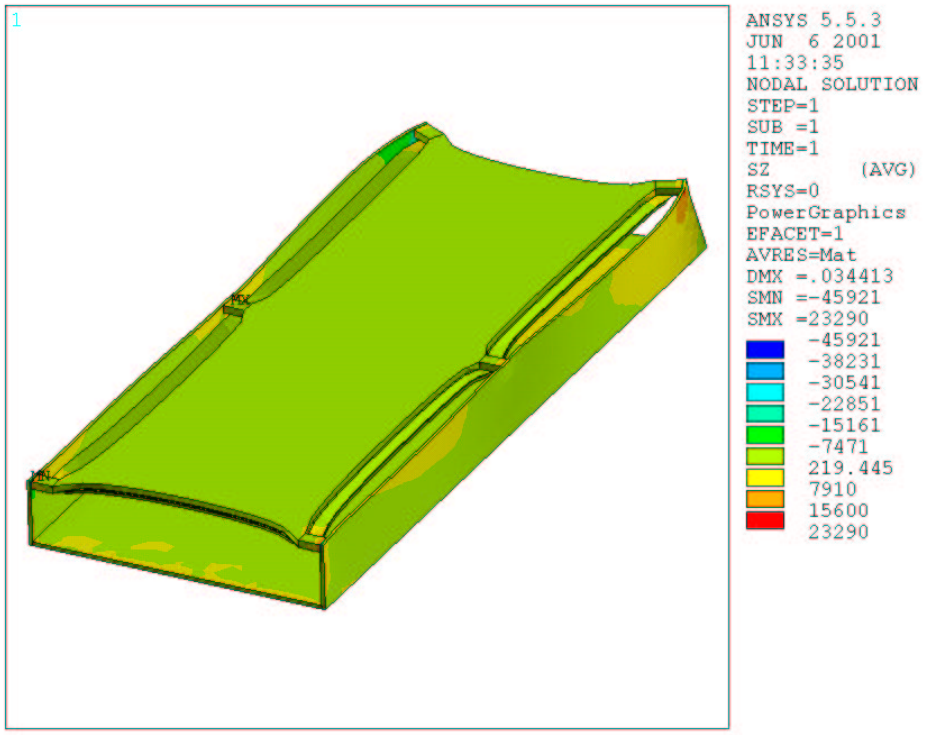

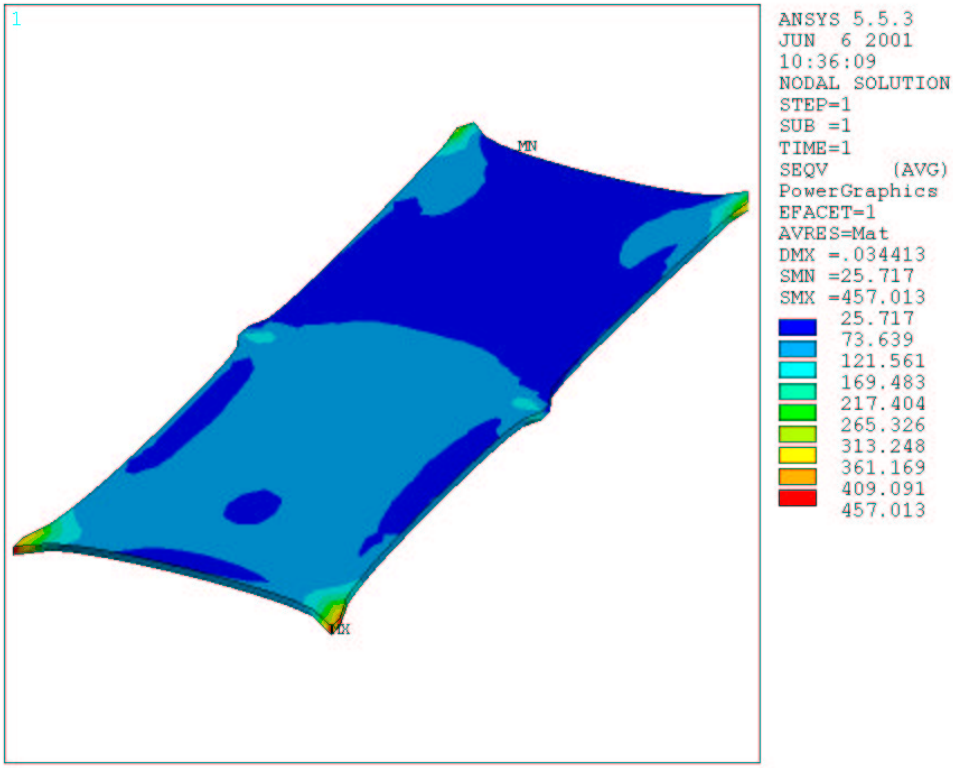

Figure 13 – From top to bottom: longitudinal stresses in half structure and Von Mises stress distribution in Rohacell [kPa, 1/7 psi] – Rohacell strength ~1600 kPa (230 psi) [Shell: K139 (90°-0°-90°-0°-90°-0°-90°); K13D2U heat spreader; Rohacell core; 6 supports]

Case	min UY	max UY	min UZ	max UZ	min stress		max stress	
	µm	µm	µm	µm	kPa	psi	kPa	psi
1	-9	0	0	10	-21148	-3066	19423	2816
2	-109	207	-10	41	-21656	-3140	20432	2963
3	-101	2	0	10	-21143	-3066	19412	2815
4	-103	0	-4	1	-36683	-5319	24081	3492
5	-44	18	-4	2	-43258	-6272	22989	3333
6	-7	6	-27	34	-45921	-6659	23290	3377

Case

1 Shell: K139 + Boron Prepreg; heat spreader perfectly matching silicon CTE

2 Shell: K139 + Boron Prepreg; KAPTON heat spreader

3 Shell: K139 + Boron Prepreg; K13D2U heat spreader

4 Shell: K139 (90°-0°-…); K13D2U heat spreader

5 Shell: K139 (90°-0°-...); K13D2U heat spreader; 6 supports

6 Shell: K139 (90°-0°-90°-...); K13D2U heat spreader; Rohacell core; 6 supports

Table 7 – Summarize on thermal mismatch finite element analysis

4.A more realistic case

The study at the previous paragraph allows identifying the better performing materials in order to produce a more realistic model (Figure 14). The model represents a chain of three sensors per side. The hybrids are located, as already mentioned, according to two different configurations: alternate (configuration #1) and facing (configuration #2). The heat load has been spread on two areas 10 x 37.2 mm^2 per hybrid, 1 mm off the hybrid edge, each area having 2.5 W heat load. The coolant bulk temperature is assumed equal to -10 °C with a film coefficient of 2000 W/mK.

In Figure 14 the modeled materials are listed and it is shown a front and isometric view of the modeled stave.

It can be seen that the temperature profile follows a similar pattern for both configurations, with a slightly lower maximum temperature for configuration 1 because of the lower heat density in the structure. Applying the temperature distribution derived from the chips heat generation, because of the lower off-set from symmetry, configuration 2 exhibits a lower vertical displacements with comparable longitudinal contraction and thermal induced stresses.

What aforementioned, can be seen in Figure 15 - Figure 20 and it is summarized in Table 8.

Component	Material
Ladder core	Rohacell
Heat spreader	K13D2U
Sensor	silicon
Outer shell	K139 [90° - 0°]
Supporting blocks	MACOR
Glue	Epoxy
Tubing	PEEK
Substrate	BeO
HDI	Kapton

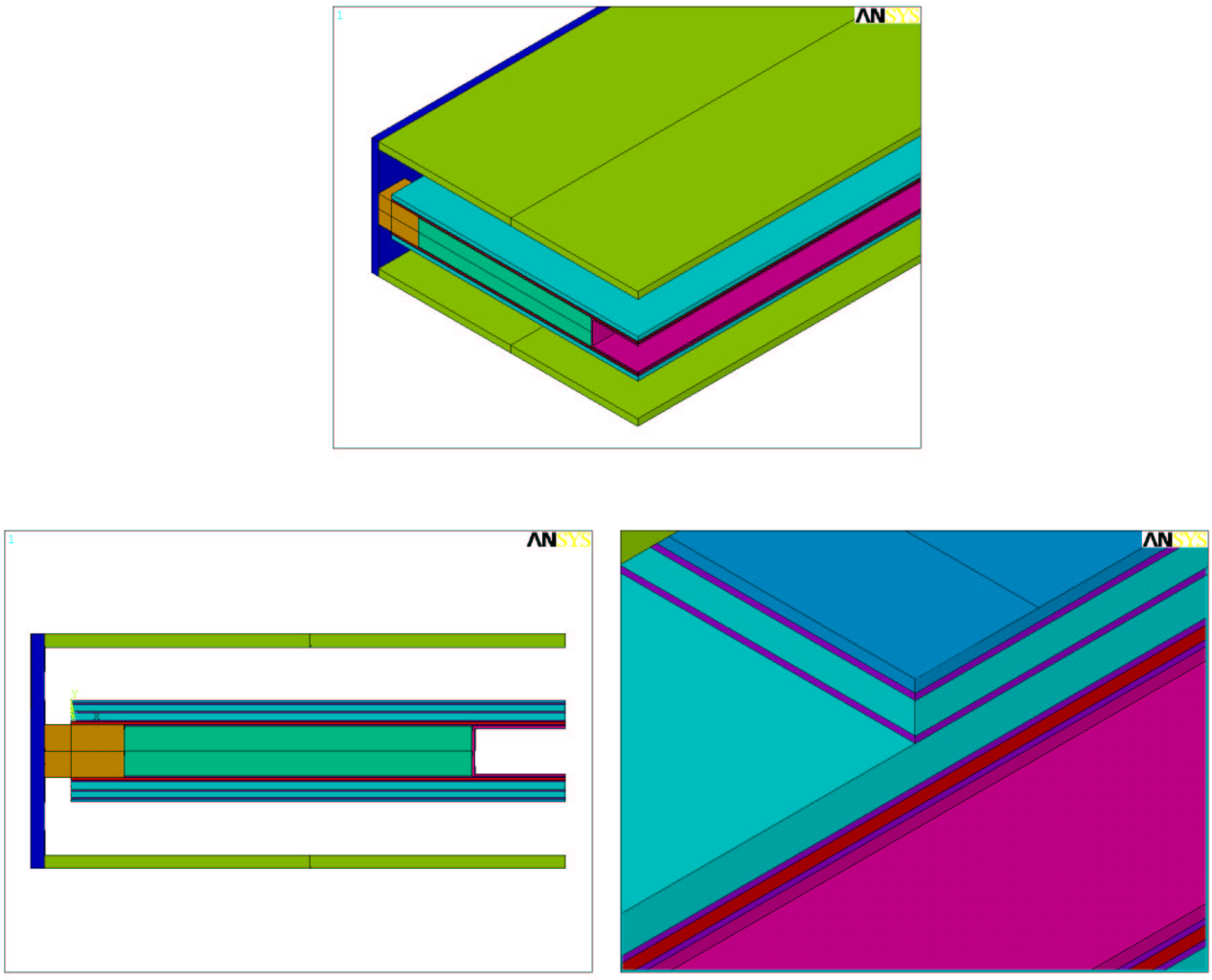

Figure 14 – Materials, isometric and front view of the detailed finite element model. Bottom right: silicon on-top mounted hybrid detail

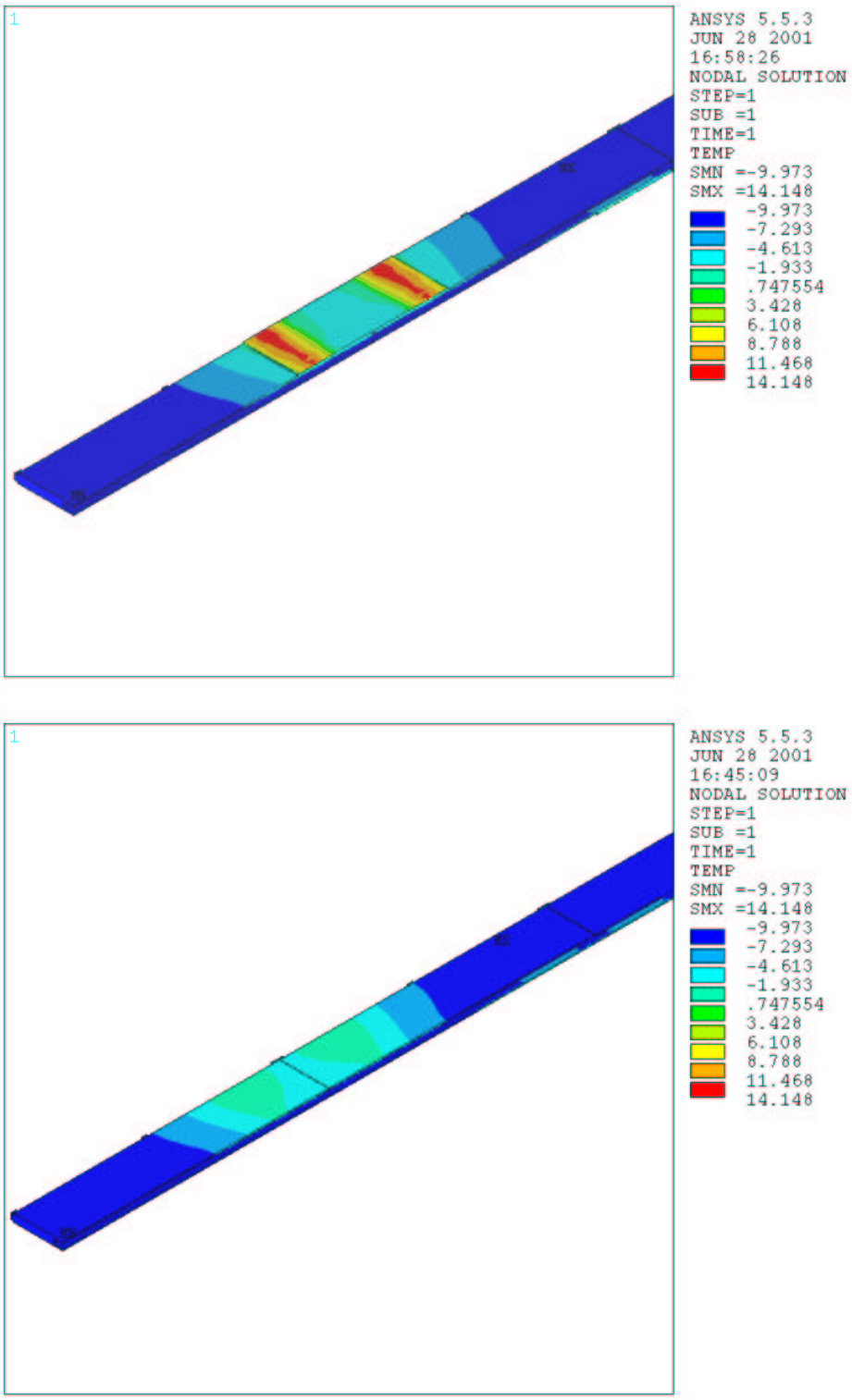

Figure 15 – Temperature distribution along three ladders with staggered hybrids. Top: hybrids detail. Bottom: silicon detail. Half structure.

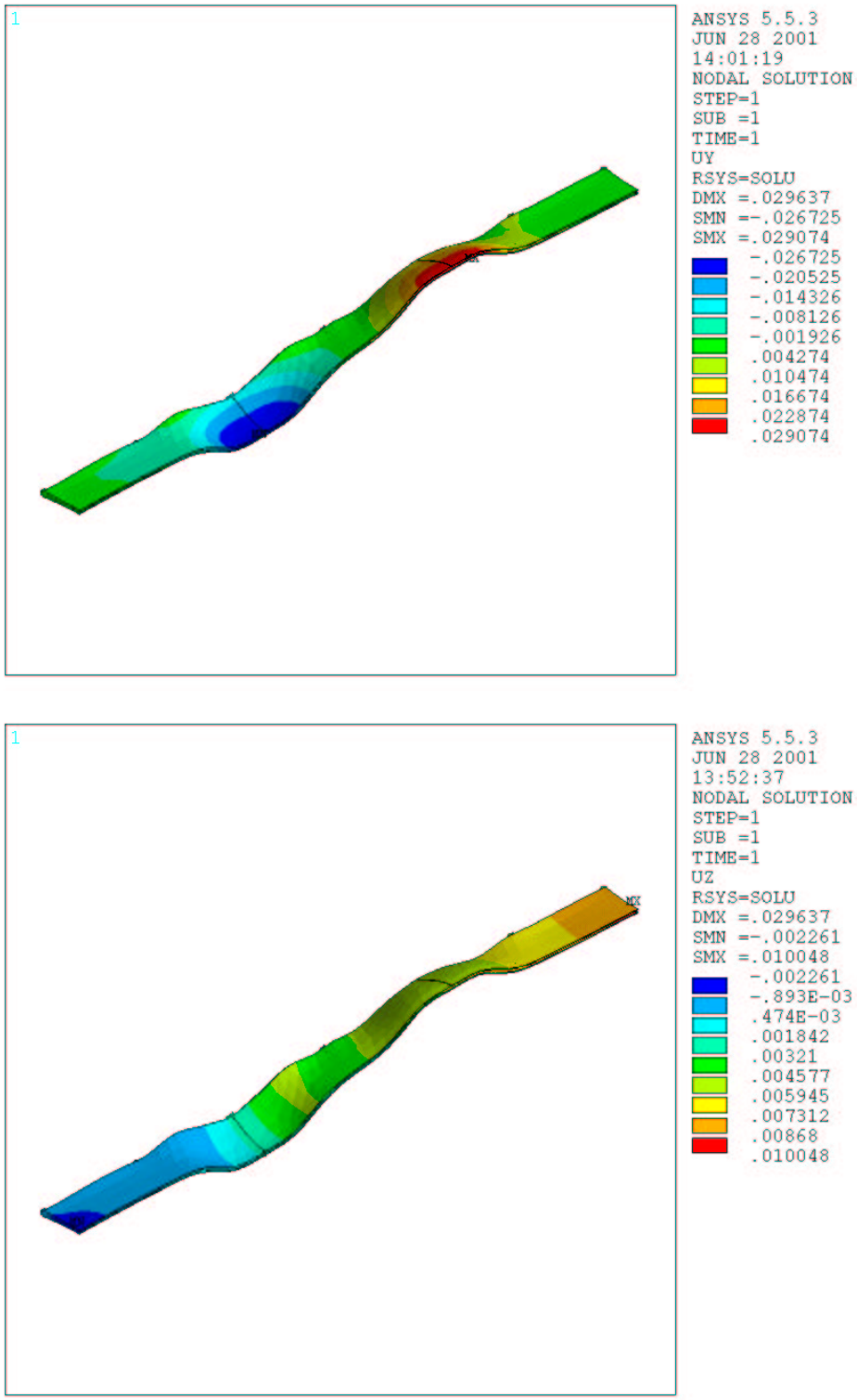

Figure 16 – From top to bottom, vertical (UY) and longitudinal (UZ) displacement in silicon due to the temperature distribution given in Figure 15. Staggered hybrids. Half structure.

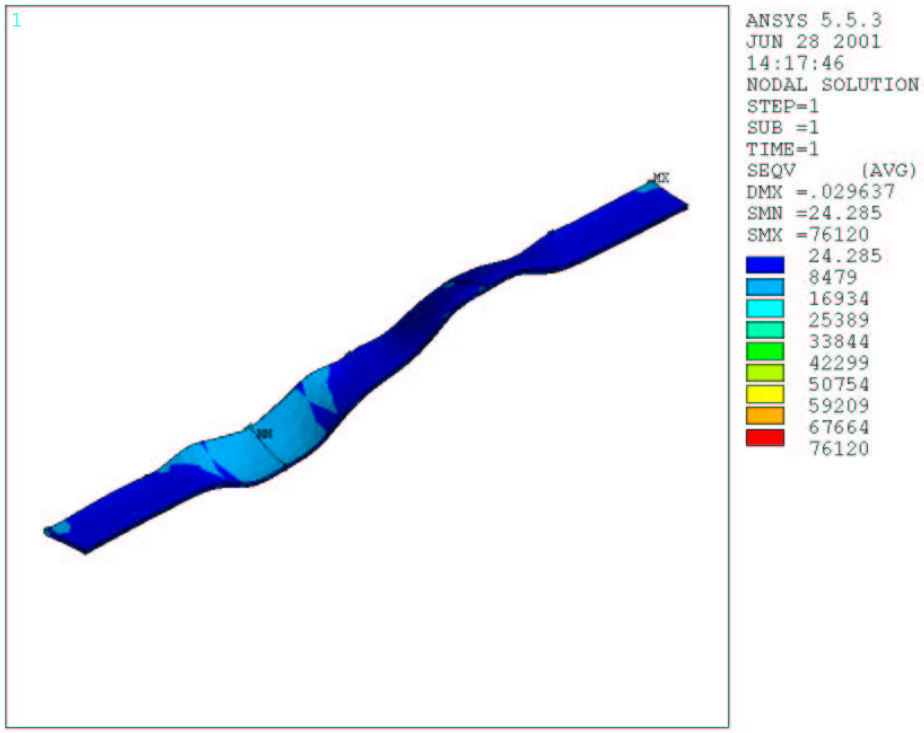

Figure 17 – Von Mises stress contour plot in silicon due to the temperature distribution given in Figure 15. Staggered hybrids. Half structure. [kPa, ~1/7 psi]

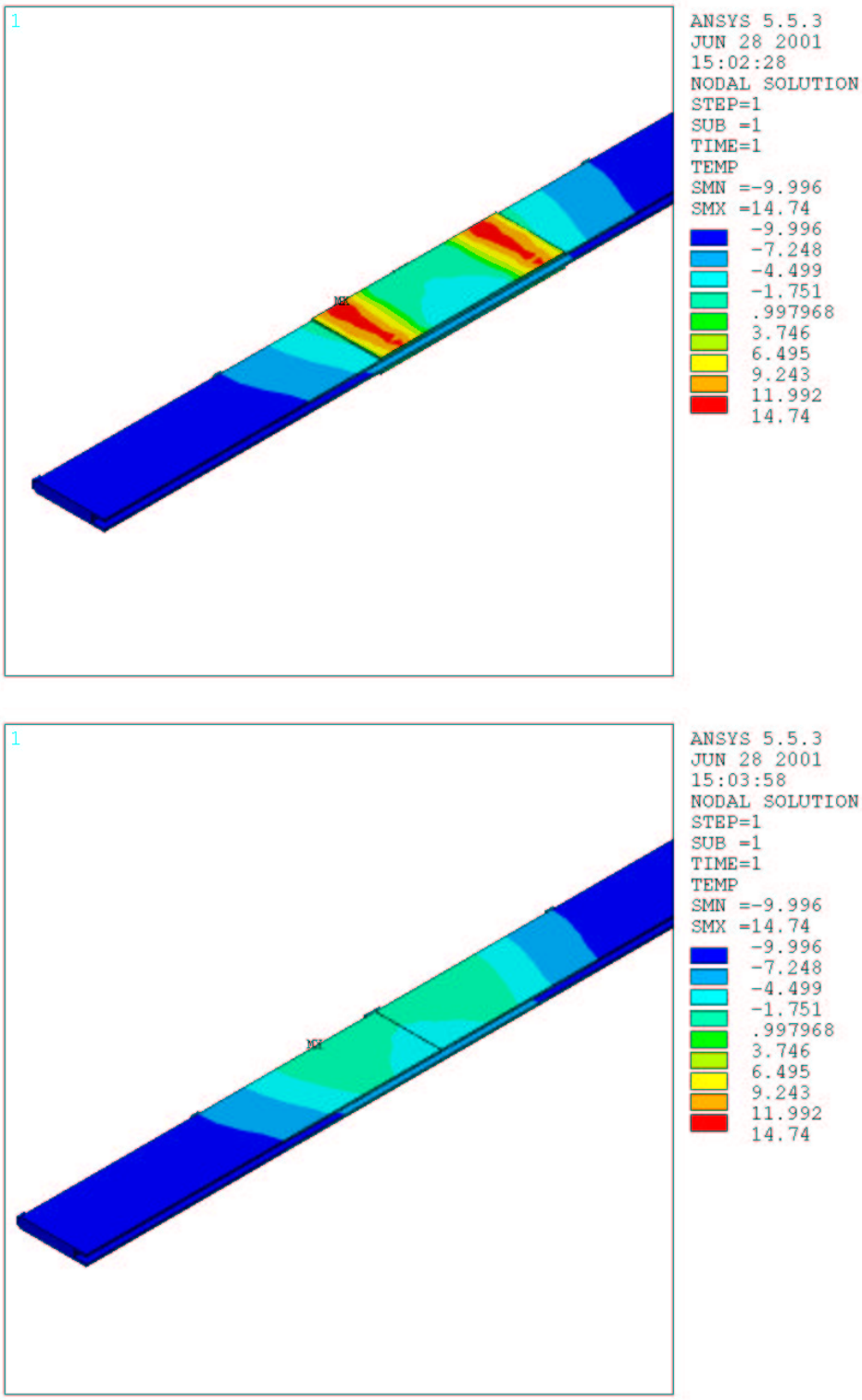

Figure 18 - Temperature distribution along three ladders with facing hybrids. Top: hybrids detail. Bottom: silicon detail. Half structure.

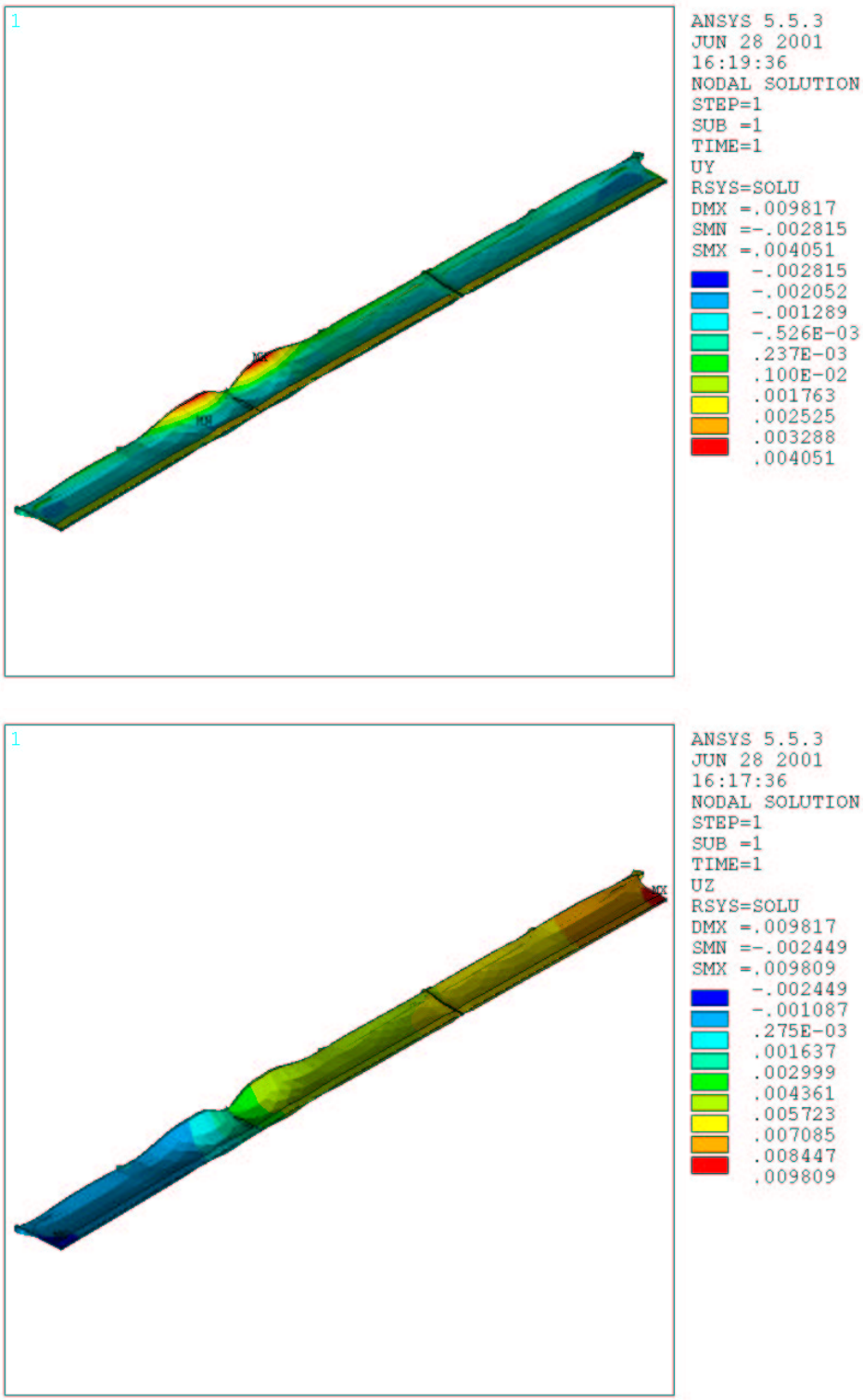

Figure 19 - From top to bottom, vertical (UY) and longitudinal (UZ) displacement in silicon due to the temperature distribution given in Figure 18. Facing hybrids. Half structure.

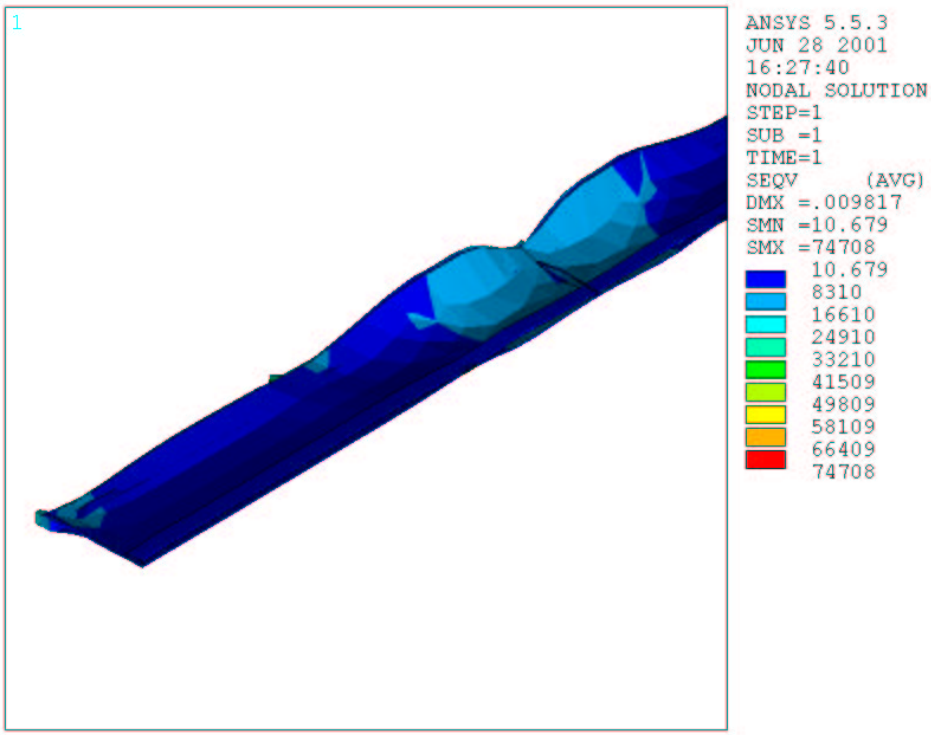

Figure 20 - Von Mises stress contour plot in silicon due to the temperature distribution given in Figure 18. Facing hybrids. Half structure. [kPa, ~1/7 psi]

case	Chip Max T	Silicon Max T	Vertical Displacement		Longitudinal Displacement		Stress (Von Mises)	
			min	max	min	max	min	max
	°C	°C	µm	µm	µm	µm	MPa	MPa
I	14.1	~0	-26	29	-2	10	0.024	76.120
II	14.7	1	-3	4	-2	10	0.010	74.708

Table 8 – Single channel staves analysis summarize

A comparison with a double cooling channel stave is reported in the following pictures and the results are summarized in Table 9. Although the structure has poorer mechanical performance, it may be preferable on the thermal standpoint, providing a considerable lower working temperature in the chip.

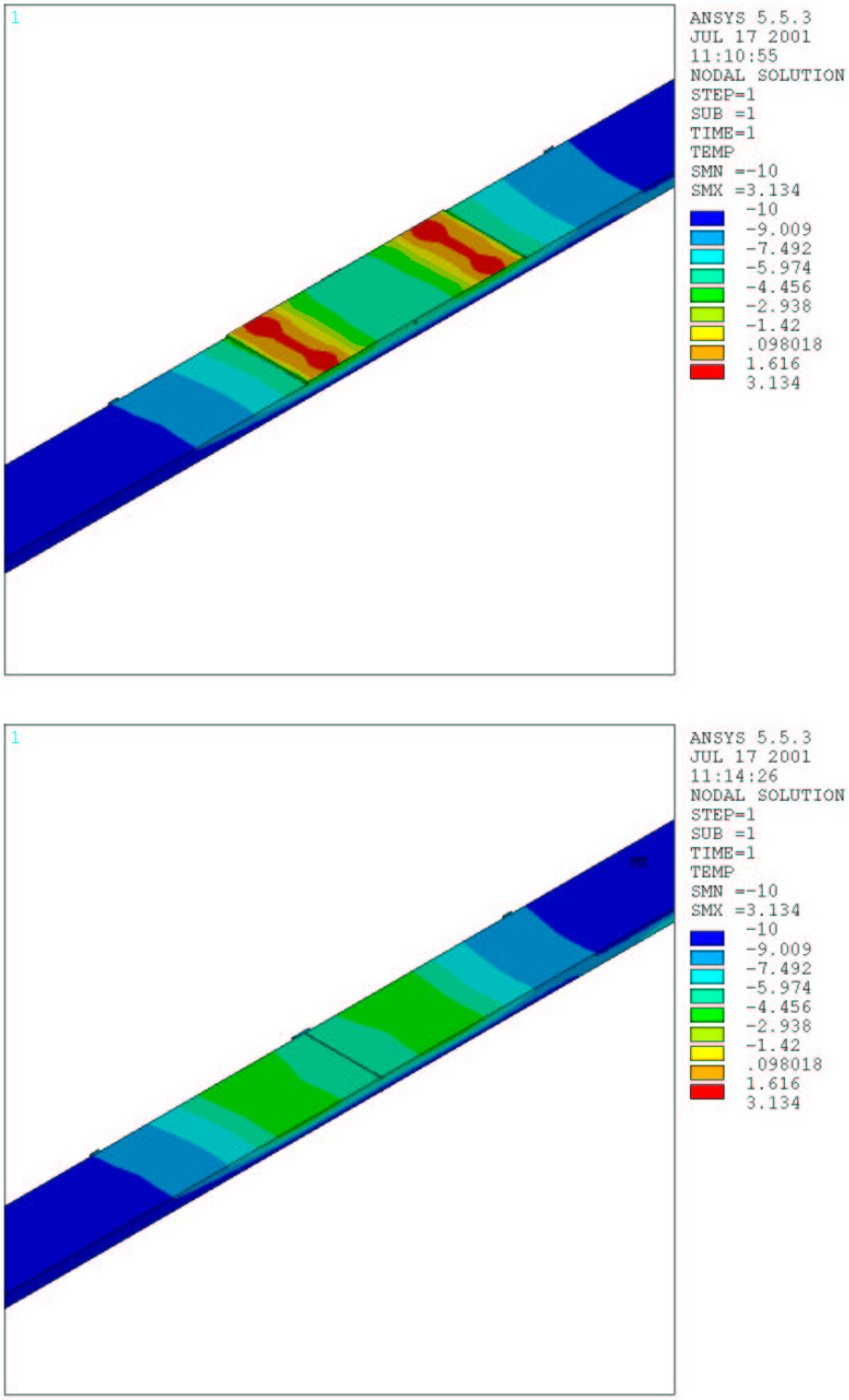

Figure 21 - Temperature distribution along three ladders with staggered hybrids. Top: hybrids detail. Bottom: silicon detail. Half structure. DOUBLE CHANNEL COOLING

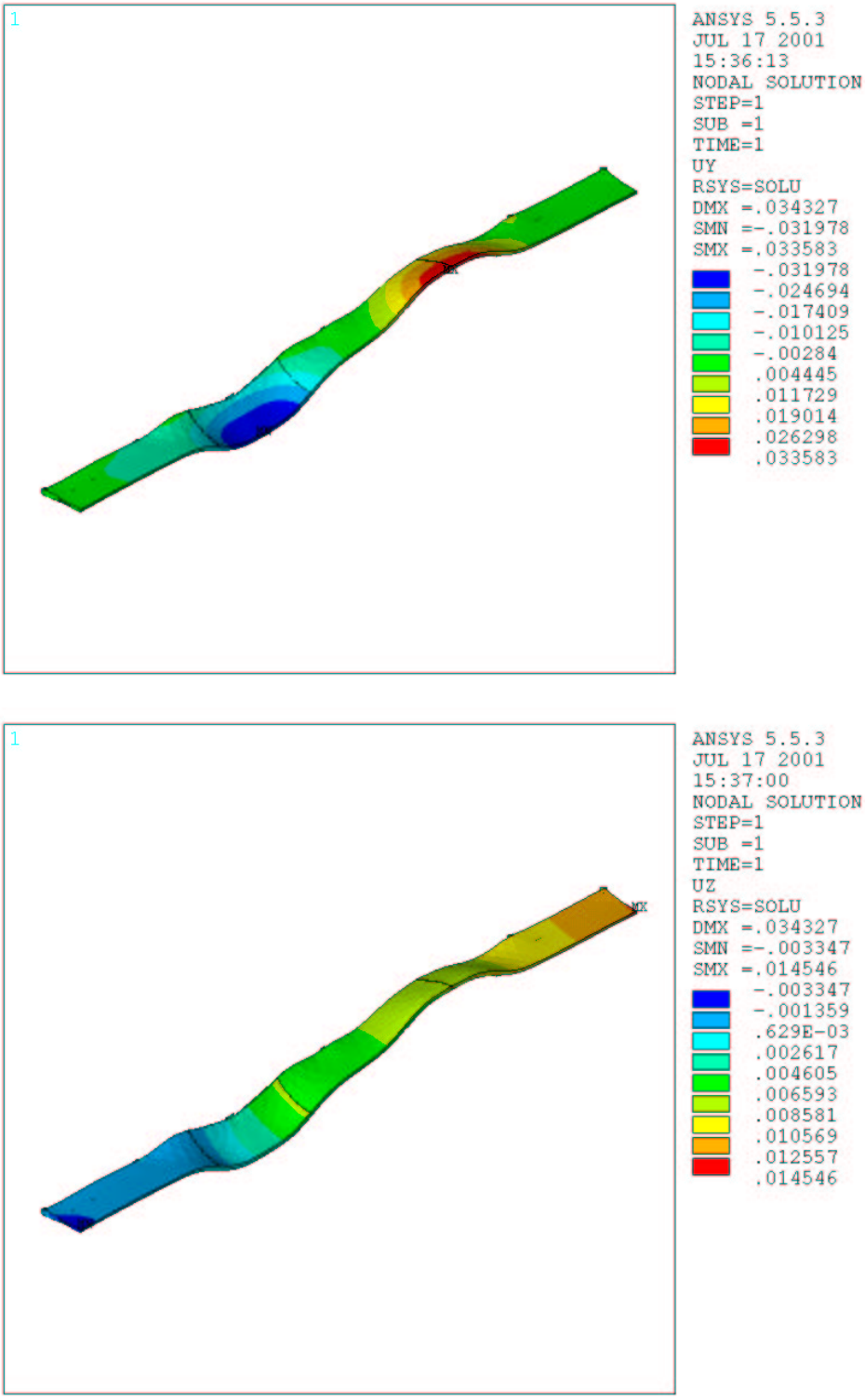

Figure 22 - From top to bottom, vertical (UY) and longitudinal (UZ) displacement in silicon due to the temperature distribution given in Figure 21. Staggered hybrids. Half structure. DOUBLE CHANNEL COOLING

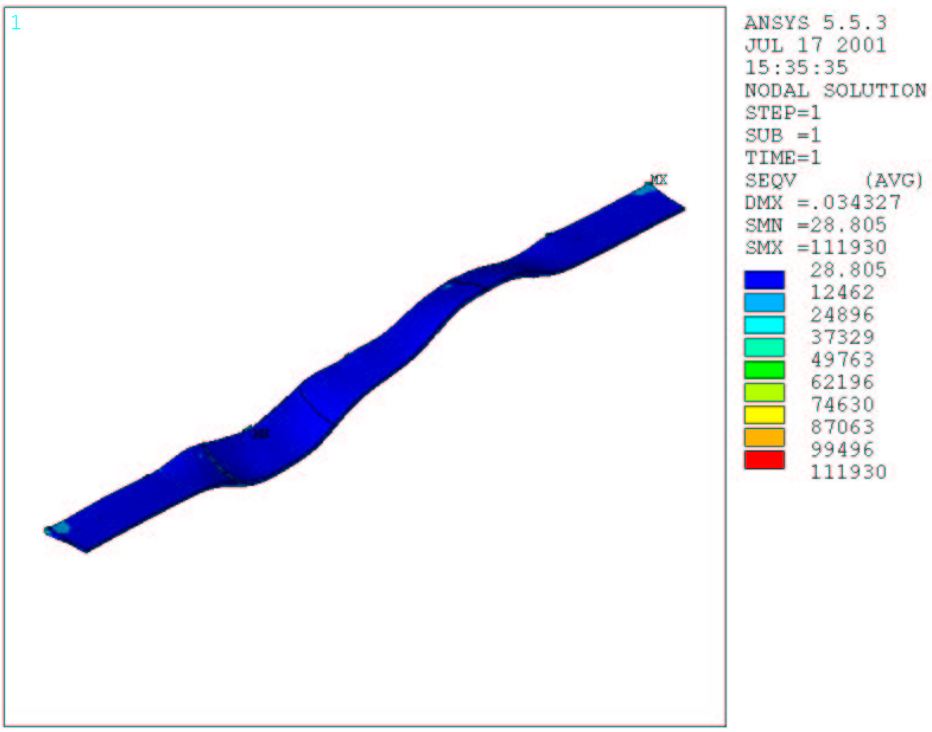

Figure 23 - Von Mises stress contour plot in silicon due to the temperature distribution given in Figure 21. Staggered hybrids. Half structure. [kPa, ~1/7 psi]. DOUBLE CHANNEL COOLING

case	Chip Max T	Silicon Max T	Vertical Displacement		Longitudinal Displacement		Stress (Von Mises)	
			min	max	min	max	min	max
	°C	°C	µm	µm	µm	µm	MPa	MPa
I	3.1	~ -2	-30	33	-3	14	0.028	112

Table 9 - Double channel staves analysis summarize

5. Conclusions

Problems related to the coefficient of thermal expansion mismatches may cause dangerous stress build-ups in the silicon sensor as well as compromise its micrometric alignment with the beam. The use of a high conductive carbon fiber heat spreader, along with a Rohacell core, may effectively help preventing the thermal bowing; at the same time, restraining the sensor from longitudinal contraction, with high modulus carbon fiber shell that does not match the silicon CTE, does not introduce dangerous stress peaks.

For the problems related to meshing a thin shell, that is poor quality elements, a further experimental study is recommended.